Journal of
Materials Chemistry B

Materials for biology and medicine
www.rsc.org/MaterialsB

ROYAL SOCIETY
OF CHEMISTRY
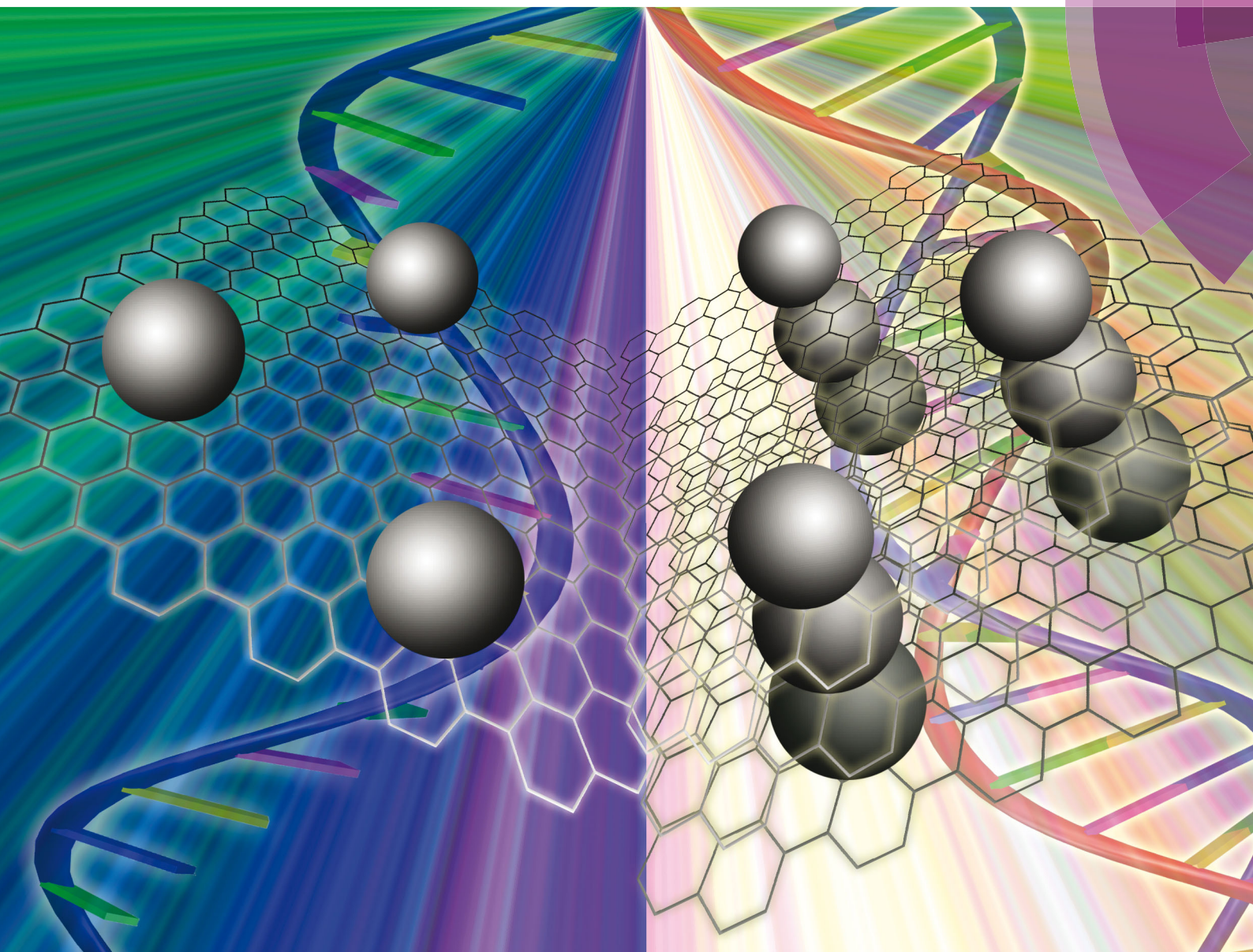
PAPER
Thomas M. H. Lee *et al.*
Platinum nanoparticles on reduced graphene oxide as peroxidase
mimetics for the colorimetric detection of specific DNA sequence

175 YEARS

PAPER

Platinum nanoparticles on reduced graphene oxide as peroxidase mimetics for the colorimetric detection of specific DNA sequence†

Li Yin Chau,[a] Qijin He,[a] Ailin Qin,[a] Shea Ping Yip[b] and Thomas M. H. Lee*[a]

In this work, we developed a simple and sensitive colorimetric detection platform for specific DNA sequences by using peroxidase mimetics of platinum nanoparticles supported on reduced graphene oxide. This nanocomposite possessed the combined advantages of platinum nanoparticles (superior peroxidase-like activity) and reduced graphene oxide (π-stacking interaction with single-stranded but not double-stranded DNA). The catalytic activity was strongly dependent on the chloroplatinic acid-to-graphene oxide mass ratio during the synthesis step, with an optimum ratio of 7:1. Unlike natural peroxidase, the nanocomposite had excellent stability over wide ranges of temperature (4–90 °C) and pH (1–13). For DNA detection, the nanocomposite had higher affinity for the single-stranded probe (in the absence of target) than the probe–target duplex. The probe-bound nanocomposite was stabilized against salt-induced aggregation and thus upon the addition of 3,3′,5,5′-tetramethylbenzidine and hydrogen peroxide to the supernatant, an intense blue color was generated. The linear range and limit of detection of this assay platform were 0.5–10 nM and 0.4 nM, respectively. Moreover, this platform featured high specificity that 3-base-mismatched sequence could be distinguished with the naked eye and 1-base-mismatched sequence with absorbance measurement. Furthermore, the applicability for real sample detection was demonstrated by polymerase chain reaction product analysis. Taken together, this new platform is well suited for point-of-care and on-site nucleic acid testing.

Introduction

Enzymes are widely used as labels for biorecognition molecules in a broad range of biosensing applications, thanks to their highly efficient catalytic properties. One of the most popular enzyme labels is horseradish peroxidase (HRP), which catalyzes the oxidation of a chromogenic substrate to yield a colored product in the presence of hydrogen peroxide (H_2O_2). The color intensity can then be correlated with the target analyte concentration. Nevertheless, the production of such a protein-based catalyst is laborious, time-consuming, and expensive. Another serious drawback is their high susceptibility to denaturation when the storage/operating conditions are not optimum (*e.g.*, high temperature and extreme pH) and thus loss of catalytic activity. In 2007, Perrett, Yan, and co-workers discovered that magnetite nanoparticles (Fe_3O_4 MNPs) possessed intrinsic peroxidase-like activity.[1] Compared with HRP, Fe_3O_4 MNPs had advantages of

simple and low-cost production as well as high stability over wide temperature and pH ranges. Since then, apart from Fe_3O_4 MNPs,[1–6] a number of nanomaterial-based enzyme mimetics have been identified,[7,8] including cerium oxide nanoparticles,[9–11] single-walled carbon nanotubes,[12] graphene oxide (GO),[13] metal nanoparticles,[14–19] and various nanocomposites.[20–29] These colorimetric reporters were successfully utilized for immunoassay[1,3,15,20,24] and detection of small-molecules (*e.g.*, glucose[2,4,13,14,18,19]) and DNA.[10–12,22,23]

For DNA detection, GO[30] and its derivatives[31] are particularly promising due to their higher binding affinity for single-stranded DNA (ssDNA; DNA probe in the absence of complementary target) than double-stranded DNA (dsDNA; probe–target duplex). The preferential binding of ssDNA is attributed to the π-stacking interaction between nucleobases and graphene while the binding of dsDNA is not favored due to the shielding of base-paired nucleobases within the duplex. Recent focus has been directed toward functionalizing GO with metal nanoparticles (*e.g.*, gold[22] and platinum[24,25,29]). These nanocomposites had considerably higher catalytic activity than GO (10-fold for gold[22] and 18-fold for platinum[24]). The nanocomposites of GO and platinum have been applied for cancer cell detection.[24,25] Park, Lee, and co-workers synthesized a nanocomposite of Fe_3O_4 and platinum nanoparticles supported on reduced GO, which was further functionalized with
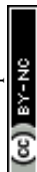
[a] *Interdisciplinary Division of Biomedical Engineering, The Hong Kong Polytechnic University, Hung Hom, Kowloon, Hong Kong, China.*
E-mail: ming-hung.lee@polyu.edu.hk; Fax: +852-23342429; Tel: +852-27664931
[b] *Department of Health Technology and Informatics,*
The Hong Kong Polytechnic University, Hung Hom, Kowloon, Hong Kong, China
† Electronic supplementary information (ESI) available: Additional data described in the text. See DOI: 10.1039/c6tb00741d

4076 | *J. Mater. Chem. B*, 2016, **4**, 4076–4083

This journal is © The Royal Society of Chemistry 2016

monoclonal antibody against human epidermal growth factor receptor 2, for the detection of breast cancer cells.[24] Chen and co-workers synthesized a folic acid-functionalized nanocomposite of platinum nanoparticles supported on GO for the detection of cancer cells *via* ligand–receptor binding (overexpression of the folate receptor on cancer cells).[25] To date, their applicability for DNA detection remains unexplored. Herein, we report a simple and sensitive colorimetric assay for specific DNA sequence by utilizing a nanocomposite of platinum nanoparticles supported on reduced graphene oxide (PtNPs/rGO).

Experimental

Synthesis of PtNPs/rGO and PtNPs

PtNPs/rGO nanocomposites were prepared using chloroplatinic acid hydrate (H_2PtCl_6; Sigma-Aldrich; other chemicals were also purchased from Sigma-Aldrich unless otherwise specified) and GO (1 g L^{-1}, 500 μL of nanographene oxide solution from Graphene Supermarket). Different H_2PtCl_6-to-GO mass ratios were used (1:1, 4:1, 7:1, and 10:1). The pH of the solution was adjusted to 10 with NaOH (1 M) and then incubated for 3 h with intermittent sonication (~1 min in every 30 min; WiseClean WUC-A01H ultrasonic cleaner, Daihan Scientific). Next, sodium borohydride ($NaBH_4$; 50 mM, 500 μL) was added dropwise under vortexing. After overnight incubation under shaking (1400 rpm), the resulting black products were centrifuged (8000 rpm for 15 min; Centrifuge 5415 D, Eppendorf) and washed with ultrapure water (18.2 MΩ cm, sterile-filtered with 0.22 μm pore size membrane; Milli-Q Advantage A10 System, Millipore; all solutions were prepared with sterile ultrapure water). The centrifugation and washing steps were repeated 3 times. The purified products were redispersed in water by sonication and stored at room temperature. PtNPs were prepared by mixing H_2PtCl_6 (3.5 mg, 500 μL) and $NaBH_4$ (5 mM, 500 μL; dropwise addition under shaking). The incubation and purification steps were identical to those of PtNPs/rGO.

Peroxidase-like activity of PtNPs/rGO

PtNPs/rGO nanocomposites of mass ratios of 1:1, 4:1, 7:1, and 10:1 (50 ng mL^{-1}, *i.e.*, 20 000-fold dilution of the original GO solution assuming negligible loss during the purification steps; note: this concentration did not account for the mass of the PtNPs), 3,3′,5,5′-tetramethylbenzidine (TMB; 0.83 mM), H_2O_2 (20 mM), and citrate buffer (50 mM, pH 5.0) were mixed and brought to a final volume of 100 μL. The absorbance at 652 nm was recorded at 1 min intervals (Ultrospec 2100 pro UV/visible spectrophotometer, GE Healthcare) and a photograph was taken at 10 min after the mixing of all components. A negative control (without PtNPs/rGO), PtNPs (0.35 μg mL^{-1}, equivalent to Pt content as 7:1 PtNPs/rGO), and GO (50 ng mL^{-1}) were included for comparison.

Instrumental analyses of PtNPs/rGO

Transmission electron microscopy (TEM) with energy-dispersive X-ray spectroscopy (EDS) was performed using a JEM-2100F field emission electron microscope (JEOL). X-ray diffraction (XRD)

analysis was carried out using a SmartLab X-ray diffractometer (Rigaku) using Cu Kα radiation (λ = 1.5418 Å) between 5° and 90° at a scan rate of 5° min^{-1}.

Kinetics of PtNPs/rGO

Two sets of experiments were performed with: (1) fixed TMB concentration (0.83 mM, unless otherwise specified) and varying concentration of H_2O_2 (15 mM–0.8 M) and (2) fixed H_2O_2 concentration (20 mM) and varying concentration of TMB (10 μM–0.83 mM). The reaction mixtures also contained PtNPs/rGO (50 ng mL^{-1}; at a mass ratio of 7:1 unless otherwise specified) and citrate buffer (50 mM, pH 5.0). The absorbance at 652 nm was recorded at 1 min intervals for 10 min after mixing all components.

Thermal and pH stabilities of PtNPs/rGO

PtNPs/rGO nanocomposites (5 μg mL^{-1}; at a mass ratio of 7:1) were incubated at different temperatures (4–90 °C) and pHs (1–13) for 1 h. Then, TMB (0.83 mM), H_2O_2 (20 mM), and citrate buffer (50 mM, pH 5.0) were added (PtNPs/rGO were diluted by 100-fold). The absorbance at 652 nm was measured at 10 min after mixing all components.

Salt-induced aggregation behavior of PtNPs/rGO and the stabilization effect of ssDNA

For salt-induced aggregation behavior, PtNPs/rGO nanocomposites (10 μg mL^{-1}; at a mass ratio of 7:1) were incubated with different concentrations of NaCl (0–0.1 M) for 3 h, followed by centrifugation at 3000 rpm for 1 min. The supernatant was collected and the absorbance at 250 nm was measured. Similar experiments were carried out with GO for comparison. For the stabilization effect of ssDNA, PtNPs/rGO nanocomposites (1 μg mL^{-1}; at a mass ratio of 7:1) were incubated with different concentrations of ssDNA (0–20 nM; 5′-TACAGTCATAGATGGTCGGTGGGAGGTGG-3′) in a buffered salt solution (5 mM Tris-HCl, 50 mM NaCl, 10 μg mL^{-1} Tween 20, pH 7.4) for 1 h, followed by centrifugation at 6000 rpm for 2 min. Then, TMB (0.83 mM), H_2O_2 (20 mM), and citrate buffer (50 mM, pH 5.0) were added to the supernatant (diluted by 5-fold). The absorbance at 652 nm was measured at 10 min after mixing all components.

Colorimetric detection of specific DNA sequence using PtNPs/rGO

Target DNA sequence (5′-CCACCTCCCACCGACCATCTATGACT GTA-3′) was hybridized with its complementary probe sequence (5′-TACAGTCATAGATGGTCGGTGGGAGGTGG-3′) at 37 °C for 1 h. After cooling to room temperature, PtNPs/rGO nanocomposites (mass ratio of 7:1) were added and the mixture was incubated for 1 h. The final concentrations of the target, probe, and PtNPs/rGO were 0–10 nM, 10 nM, and 1 μg mL^{-1}, respectively. The hybridization and incubation were carried out under buffered salt conditions (5 mM Tris-HCl, 50 mM NaCl, and 10 μg mL^{-1} Tween 20, pH 7.4). This was followed by centrifugation at 6000 rpm for 2 min. After then, TMB (0.83 mM), H_2O_2 (20 mM), and citrate buffer (50 mM, pH 5.0) were added to the supernatant (diluted by 5-fold). The absorbance

This journal is © The Royal Society of Chemistry 2016

J. Mater. Chem. B, 2016, **4**, 4076–4083 | **4077**

at 652 nm was recorded at 1 min intervals for 10 min after mixing all components and a photograph was taken at 10 min. For specificity test, the target sequence was substituted by 1-base-mismatched (5′-CCACCTCCCACCGAGCATCTATGACTGTA-3′) or 3-base-mismatched (5′-CCACCTCCCACCGTGGATCTATGACTGTA-3′) sequences.

For polymerase chain reaction (PCR) product detection, PCR samples were prepared with $1\times$ standard Taq reaction buffer (10 mM Tris-HCl, 50 mM KCl, 1.5 mM $MgCl_2$, pH 8.3), dNTPs (0.1 mM each), Primer 1 (5′-CTGCTCCTGTTGAGTTTATTGC-3′, 0.4 μM), Primer 2 (5′-GCGAACAATTCAGCGGCTTTA-3′, 0.4 μM), Taq DNA polymerase (0.025 units μL^{-1}), and the target ($\phi \times 174$ for a positive sample, 5 pg μL^{-1}; water for a negative sample). The PCR reagents were purchased from New England Biolabs except the primers were purchased from Integrated DNA Technologies. Thermal cycling was carried out using GeneAmp PCR system 9700 (Applied Biosystems) and the profile used was 94 °C for 2 min (initial denaturation); 35 cycles of 94 °C for 15 s (denaturation), 55 °C for 15 s (annealing), and 72 °C for 30 s (extension); and 72 °C for 2 min (final extension). After cooling to room temperature, the PCR samples (80-fold dilution; equivalent to 10 nM total initial primer concentration) were added to PtNPs/rGO nanocomposites. Subsequent steps and conditions were identical to those used for the 29-base target in the previous paragraph. Dynamic light scattering (DLS) analysis was performed using a Zetasizer Nano ZS (Malvern; 633 nm He–Ne laser) to investigate the dispersion/aggregation of the PtNPs/rGO nanocomposites upon the addition of PCR samples.

Results and discussion

Peroxidase-like activity of PtNPs/rGO

The peroxidase-like activity of the PtNPs/rGO nanocomposites was confirmed by their ability to catalyze the oxidation of TMB with H_2O_2 as the oxidizing agent. As expected, the solution turned from colorless to blue (Fig. 1A). For the sample without PtNPs/rGO (negative control) or with GO, the solution remained colorless. Besides visual evaluation, the blue-colored product formation was monitored by visible absorbance measurements (Fig. S1, ESI;† peak absorbance at 652 nm). Fig. 1B shows the real-time monitoring of the TMB oxidation catalyzed by the PtNPs/rGO nanocomposites of different H_2PtCl_6-to-GO mass ratios (1:1, 4:1, and 7:1). Importantly, the catalytic activity was strongly dependent on the H_2PtCl_6-to-GO mass ratio, with an optimum ratio of 7:1 (Fig. S2, ESI†). Furthermore, the catalytic activity was strongly pH dependent (highest at pH 5; Fig. S3, ESI†).

Instrumental analyses of PtNPs/rGO

Transmission electron microscopy (TEM) photographs showed that the higher the mass ratio, the greater the amount of PtNPs (Fig. 2). The size of the PtNPs for the 1:1, 4:1, and 7:1 nanocomposites was mostly 4–5 nm while that of the 10:1 nanocomposites was larger (Fig. S4, ESI;† reduced effective surface area and thus lower catalytic activity compared with
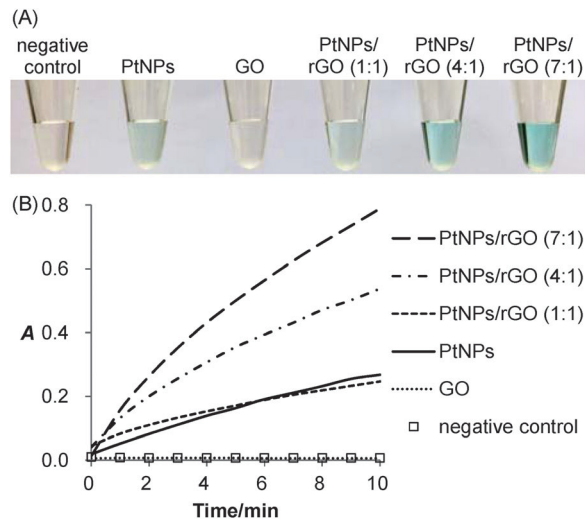

Fig. 1 Peroxidase-like activity of platinum nanoparticles supported on reduced graphene oxide (PtNPs/rGO). (A) Photograph showing the colorimetric responses of (from left to right) 3,3′,5,5′-tetramethylbenzidine (TMB) and H_2O_2 alone (negative control), and in the presence of platinum nanoparticles (PtNPs), graphene oxide (GO), as well as PtNPs/rGO of 1:1, 4:1, and 7:1 mass ratios. The concentrations of TMB, H_2O_2, and PtNPs/rGO were 0.83 mM, 20 mM, and 50 ng mL^{-1}, respectively. For PtNPs and GO, the concentrations were equivalent to the corresponding amounts of PtNPs/rGO at a 7:1 mass ratio. The photograph was taken at 10 min after mixing all components. (B) Plots of absorbance at 652 nm versus time for the samples in (A).
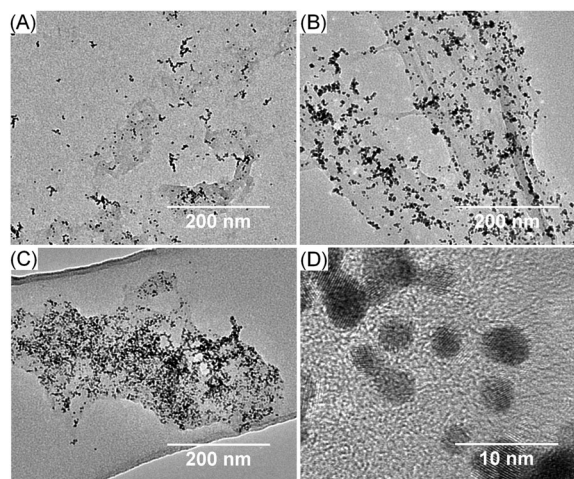

Fig. 2 Transmission electron microscopy (TEM) photographs of PtNPs/rGO of different mass ratios: (A) 1:1; (B) 4:1; and (C and D) 7:1 at low and high magnification.

7:1 nanocomposites). Indeed, GO played a crucial role in synthesizing the small-sized PtNPs. Without GO (same amount of H_2PtCl_6 as the 7:1 PtNPs/rGO nanocomposites), the size of the PtNPs was substantially larger (not shown), the catalytic activity of which was significantly lower than that of the 7:1 PtNPs/rGO nanocomposites (Fig. 1). EDS analysis was performed to further confirm the formation of the 7:1 PtNPs/rGO nanocomposites (Fig. S5, ESI†). The EDS spectrum of the
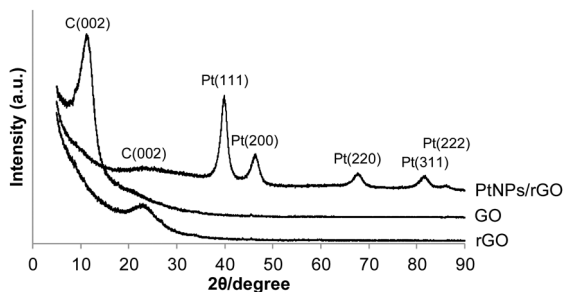
4078 | J. Mater. Chem. B, 2016, 4, 4076–4083

This journal is © The Royal Society of Chemistry 2016

Fig. 3 XRD pattern of PtNPs/rGO (mass ratio of 7:1). GO and rGO were included for comparison.

PtNPs/rGO nanocomposites shows the corresponding peaks of the C, O, and Pt elements, indicating the deposition of PtNPs on rGO. In comparison, the peak corresponding to the O element is absent in the EDS spectra of the PtNPs alone and the background (carbon film supported on a copper grid).

The XRD patterns of the 7:1 PtNPs/rGO nanocomposites, GO, and rGO are shown in Fig. 3. For GO, a diffraction peak at $11.4°$ corresponding to the C(002) plane is observed.[32–34] This peak shifts to $22.8°$ after the reduction treatment by $NaBH_4$ (pattern of rGO) due to the removal of the hydroxyl, epoxy, and carboxyl groups which exist between GO layers.[32–34] The C(002) peak of the PtNPs/rGO nanocomposites is at $23.3°$, which is close to that of rGO. The XRD pattern of the PtNPs/rGO nanocomposites exhibits diffraction peaks corresponding to

the (111), (200), (220), (311), and (222) planes of the face-centered cubic (fcc) Pt lattice,[33–35] indicating the crystalline state of the PtNPs. Based on the Pt(220) diffraction peak, the size of the PtNPs was determined to be 5.3 nm using the Scherrer equation, which is consistent with the TEM result.

Kinetics of PtNPs/rGO

Kinetic experiments were carried out to investigate the relationship between the initial velocity of the 7:1 PtNPs/rGO-catalyzed reaction and the substrate concentration. Using H_2O_2 as the substrate (TMB concentration was fixed at 0.83 mM), a linear relationship was obtained over the concentration range studied (15 mM–0.8 M; Fig. 4A). Using TMB as the substrate (H_2O_2 concentration was fixed at 20 mM), a hyperbolic curve (typical for the Michaelis–Menten kinetic model: $v_0 = V_{max}[S]/(K_M + [S])$, where v_0 is the initial velocity, V_{max} is the maximal velocity, K_M is the Michaelis Menten constant, and $[S]$ is the substrate concentration) was obtained between 0 and 0.2 mM (Fig. 4B). It should be noted that higher TMB concentrations inhibited the catalytic activity. Such substrate inhibition was also observed in a previous study.[29] To obtain the kinetic parameters, the data were represented as double-reciprocal plots (i.e., $1/v_0$ versus $1/[S]$, the Lineweaver–Burk plots; x-intercept = $-1/K_M$ and y-intercept = $1/V_{max}$). The apparent K_M values using TMB and H_2O_2 as the substrates were calculated to be 80.6 μM (data in Fig. 4B; TMB concentrations of 10 μM–0.1 mM) and 0.935 M (data in Fig. 4C), respectively, which correspond to the substrate concentrations at $V_{max}/2$ (often a rough indication of the affinity for

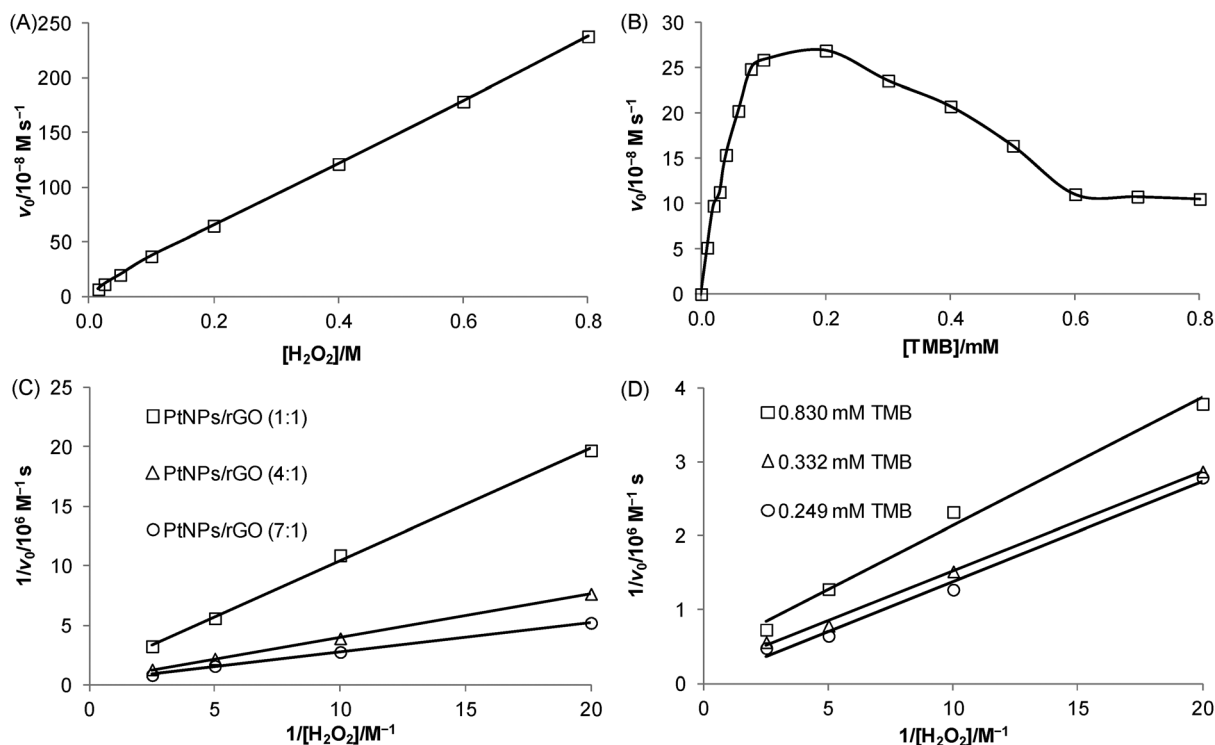**Fig. 4** Kinetics of PtNPs/rGO (mass ratio of 7:1 unless otherwise specified; the concentration was 50 ng mL^{-1}). (A) Plot of initial velocity versus H_2O_2 concentration at a fixed TMB concentration of 0.83 mM. (B) Plot of initial velocity versus TMB concentration at a fixed H_2O_2 concentration of 20 mM. (C) Double-reciprocal plots of initial velocity versus H_2O_2 concentration at a fixed TMB concentration of 0.83 mM for PtNPs/rGO of 1:1, 4:1, and 7:1 mass ratios. (D) Double-reciprocal plots of initial velocity versus H_2O_2 concentration at 3 different fixed TMB concentrations (0.249, 0.332, and 0.830 mM).

This journal is © The Royal Society of Chemistry 2016

J. Mater. Chem. B, 2016, **4**, 4076–4083 | **4079**

Table 1 Kinetic parameters of PtNPs/rGO and HRP

	TMB as substrate		H$_2$O$_2$ as substrate	
	K_M/mM	$V_{max}/10^{-8}$ M s^{-1}	K_M/mM	$V_{max}/10^{-8}$ M s^{-1}
PtNPs/rGO[a]	0.0806	46.5	935	378
HRP[1]	0.434	10.0	3.70	8.71

[a] The mass ratio of PtNPs/rGO was 7:1. The apparent kinetic parameters with TMB as a substrate were calculated from the data in Fig. 4B (TMB concentration from 10 μM to 0.1 mM) and those with H$_2$O$_2$ as a substrate were calculated from the data in Fig. 4C.

the substrate). A comparison of the kinetic parameters of the 7:1 PtNPs/rGO nanocomposites with those of HRP and nanomaterial-based peroxidase mimetics reported in the literature is given in Table 1 and Table S1 (ESI†). Fig. 4C shows the double-reciprocal plots of the 7:1, 4:1, and 1:1 PtNPs/rGO nanocomposites with H$_2$O$_2$ as the substrate. From the intercepts, the apparent V_{max} values increased with increasing mass ratio while the apparent K_M values were the same for the 3 nanocomposites. To investigate the binding mechanism of this 2-substrate reaction (*i.e.*, ping–pong or ternary-complex mechanism), double-reciprocal plots of the 7:1 PtNPs/rGO nanocomposites with H$_2$O$_2$ as the substrate were obtained at 3 different fixed TMB concentrations (Fig. 4D). The resulting lines were parallel, indicating a ping–pong mechanism

Fig. 6 Salt-induced aggregation behavior of PtNPs/rGO (mass ratio of 7:1) as well as stabilization effect by single-stranded DNA (ssDNA). (A) PtNPs/rGO nanocomposites (10 μg mL^{-1}) were incubated with different concentrations of NaCl for 3 h. The aggregated nanocomposites were precipitated by centrifugation and the amount of nanocomposites that remained dispersed in the supernatant was determined by absorbance measurement at 250 nm. GO was included for comparison. (B) PtNPs/rGO nanocomposites (1 μg mL^{-1}) were incubated with different concentrations of ssDNA for 1 h in the presence of 50 mM NaCl, followed by centrifugation to precipitate the aggregated nanocomposites. The dispersed nanocomposites in the supernatant (diluted 5-fold) were mixed with TMB (0.83 mM) and H$_2$O$_2$ (20 mM) for color development. The absorbance at 652 nm was taken at 10 min after mixing all components.
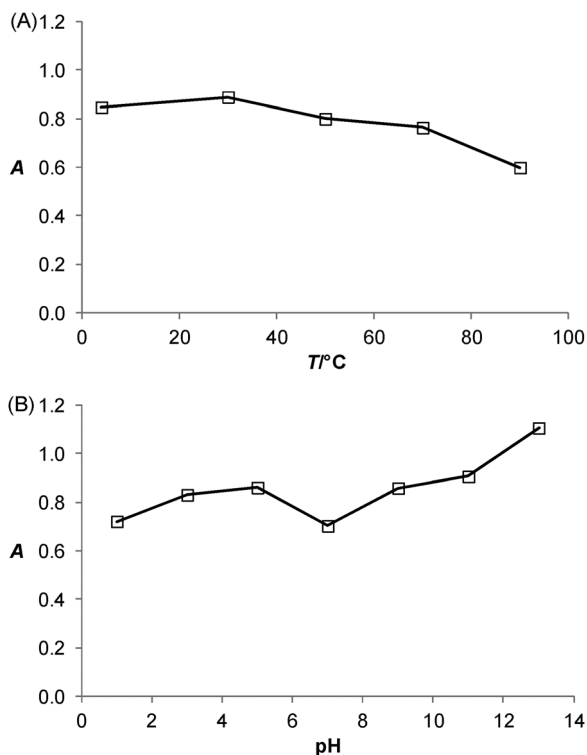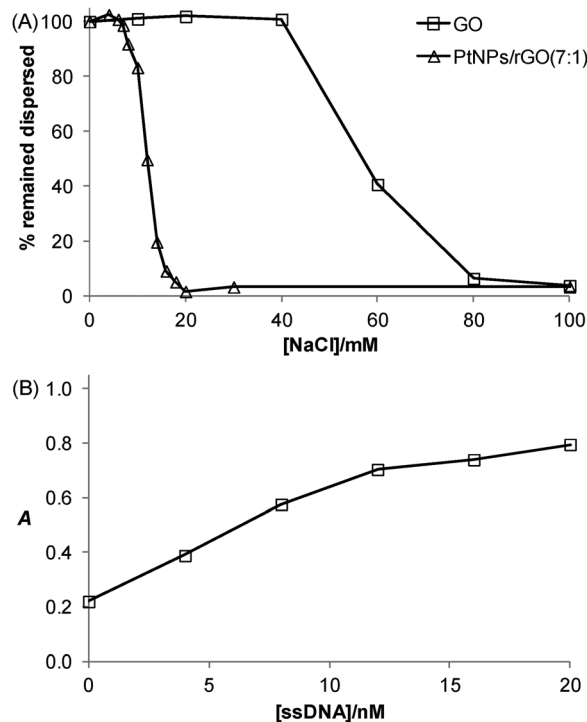

Fig. 5 (A) Thermal and (B) pH stabilities of PtNPs/rGO. PtNPs/rGO nanocomposites (mass ratio of 7:1) were first incubated at a particular temperature or pH for 1 h. Then, TMB (0.83 mM) and H$_2$O$_2$ (20 mM) were added. The final concentration of PtNPs/rGO was 50 ng mL^{-1} and the pH was adjusted to 5.0. The reaction was allowed to proceed at room temperature and the absorbance at 652 nm was taken at 10 min after mixing all components.

(*i.e.*, one substrate first binds with the catalyst and is released to give an intermediate catalyst, followed by the binding of the second substrate).
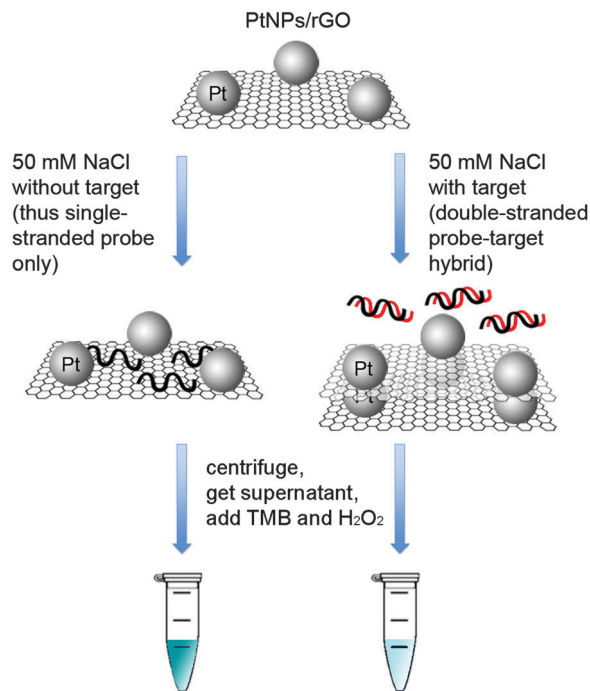
Thermal and pH stabilities of PtNPs/rGO

The effects of incubation temperature and pH on the catalytic activity of the PtNPs/rGO nanocomposites were studied. Fig. 5 shows the thermal and pH stabilities of the PtNPs/rGO nanocomposites. The catalytic activity was well preserved even after 1 h of incubation over wide temperature (4–90 °C) and pH (1–13) ranges. These compare favorably with those of HRP, which remained catalytically active only at incubation temperatures below 45 °C and pH 6–11.[1]

Salt-induced aggregation behavior of PtNPs/rGO and the stabilization effect of ssDNA

The salt-induced aggregation property along with the stabilization effect exerted by ssDNA is a useful strategy for GO- or rGO-based detection of specific DNA sequence.[31] Fig. 6A shows that the PtNPs/rGO nanocomposites remained fully dispersed up to 6 mM

4080 | *J. Mater. Chem. B*, 2016, **4**, 4076–4083

This journal is © The Royal Society of Chemistry 2016

Scheme 1 Schematic illustration of the colorimetric detection of specific DNA sequence using the PtNPs/rGO nanocomposites. (Left tube) without target: intense blue; (right tube) with target: pale blue.
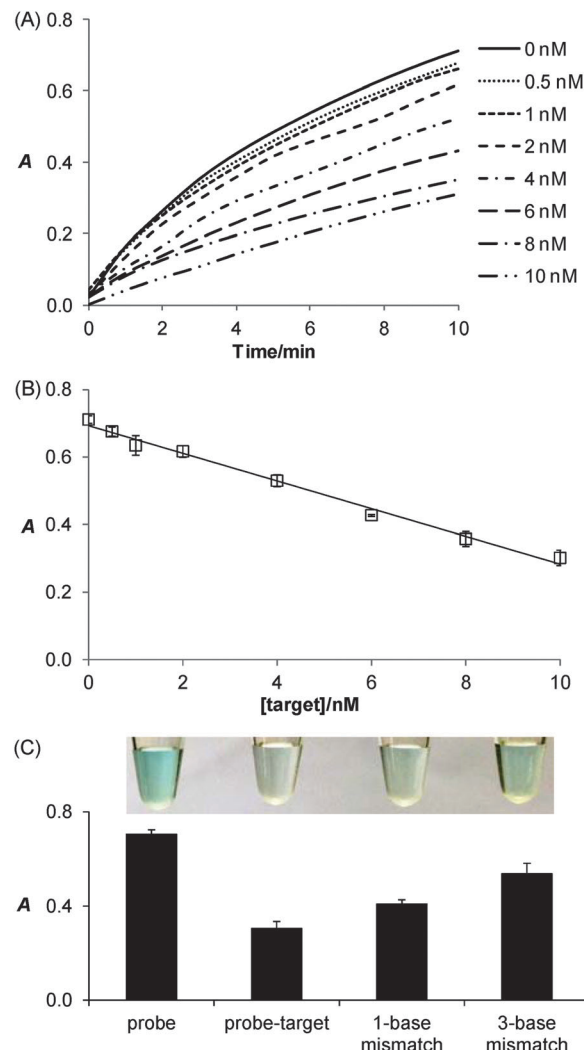

Fig. 7 PtNPs/rGO for the colorimetric detection of specific DNA sequence. (A) Plots of absorbance at 652 nm versus time for different concentrations (0, 0.5, 1, 2, 4, 6, 8, and 10 nM) of the target sequence. The concentrations of PtNPs/rGO (mass ratio of 7 : 1) and the probe were 1 μg mL^{-1} and 10 nM, respectively. After 1 h of incubation followed by centrifugation, TMB and H$_2$O$_2$ were added to the supernatant (final concentrations of 0.83 mM and 20 mM, respectively). (B) Plots of absorbance at 652 nm (10 min after the addition of TMB and H$_2$O$_2$) versus concentration of the target sequence. (C) Specificity test showing the differentiation of 1-base-mismatched and 3-base-mismatched sequences from the full-matched target based on absorbance measurement and visual readout (taken at 10 min after the addition of TMB and H$_2$O$_2$). The concentration of the mismatched sequences was 10 nM. All other conditions were identical to those in (A).

NaCl while aggregated severely at 20 mM NaCl or higher. It should be noted that the PtNPs/rGO nanocomposites had lower salt stability than GO (remained fully dispersed up to 40 mM NaCl while aggregated severely at 80 mM NaCl or higher), which can be explained by the less negative surface charge after the NaBH$_4$ reduction process due to the removal of the edge oxygen-containing groups (i.e., carboxyl and phenolic hydroxyl).[32] One facile and efficient way to prevent salt-induced aggregation of the PtNPs/rGO nanocomposites is by ssDNA stabilization. The binding of ssDNA to rGO through π-stacking interaction renders additional negative charge, thereby allowing the PtNPs/rGO nanocomposites to remain dispersed at high NaCl concentrations. For example, when the PtNPs/rGO nanocomposites were mixed with a sufficient amount of ssDNA in the presence of 50 mM NaCl, after incubation and centrifugation, the ssDNA-stabilized nanocomposites in the supernatant exhibited a strong catalytic activity. More specifically, with 1 μg mL^{-1} PtNPs/rGO, the stabilization effect increased linearly with increasing ssDNA concentration up to 10 nM (Fig. 6B). At higher concentrations, the curve leveled off as a result of the saturation of ssDNA on the PtNPs/rGO surface.

Colorimetric detection of specific DNA sequence using PtNPs/rGO

Taking advantage of the ssDNA-controlled and salt-induced aggregation property as well as the ultrahigh peroxidase-like catalytic activity of the PtNPs/rGO nanocomposites, we developed a simple and sensitive platform for the colorimetric detection of specific DNA sequence (Scheme 1). The assay starts with the

hybridization of a target sequence with its complementary probe sequence, followed by the addition of the PtNPs/rGO nanocomposites. In the absence of the target, the PtNPs/rGO nanocomposites bind with the single-stranded probe and are stabilized against aggregation at 50 mM NaCl. After centrifugation, the supernatant, which contains a large amount of nanocomposites, is added to TMB and H$_2$O$_2$, giving rise to an intense blue color. On the other hand, the PtNPs/rGO nanocomposites do not bind with the double-stranded probe–target
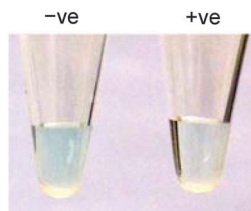
Fig. 8 Colorimetric detection of the PCR product using PtNPs/rGO: (left) negative sample and (right) positive sample.

hybrid and thus undergo aggregation at 50 mM NaCl. The supernatant, which contains a small amount of nanocomposites, results in a pale blue color upon the addition of TMB and H_2O_2. Plots of absorbance at 652 nm *versus* time for different target concentrations (0–10 nM; the probe concentration was 10 nM) were obtained (Fig. 7A). The absorbance value at 10 min decreased linearly with increasing target concentration (Fig. 7B). The limit of detection was determined to be 0.4 nM (based on 3 times the standard deviation of the blank), which compares favorably with other previously reported enzyme mimetics.[12,22,23] Furthermore, the ability to distinguish mismatched sequences from the full-matched target was evaluated. Fig. 7C shows that the absorbance values of the 1-base-mismatched and 3-base-mismatched sequences were significantly higher than those of the full-matched target (35% and 77%, respectively). In fact, the 3-base-mismatched sequence was clearly distinguishable from the full-matched target with the naked eye.

We further utilized the platform for PCR product detection (Fig. 8). An aliquot of the PCR product (uncleaned sample, *i.e.*, without post-PCR cleanup of dNTPs and enzyme) was mixed with the PtNPs/rGO nanocomposites in 50 mM NaCl. For the negative sample (without target; in this case $\phi \times 174$), the primers remained as a single-stranded state and stabilized the PtNPs/rGO nanocomposites against salt-induced aggregation. As a result, a blue color was observed upon the addition of TMB and H_2O_2 to the supernatant. For the positive sample (with target), the primers were extended to form a double-stranded amplicon, which could not stabilize the PtNPs/rGO nano-composites against salt-induced aggregation (supported by DLS analysis; Fig. S6, ESI†). Thus, a very light blue color was observed upon the addition of TMB and H_2O_2 to the supernatant. The ability to detect uncleaned samples suggests that dNTPs and enzyme do not affect the stabilization of PtNPs/rGO by the primers in the negative sample as well as the aggregation of PtNPs/rGO in the positive sample.

Conclusions

To conclude, we have developed a simple and sensitive colori-metric detection platform for specific DNA sequence based on PtNPs/rGO nanocomposites. These nanocomposites possessed the combined advantages of PtNPs (superior peroxidase-like activity) and rGO (preferential binding with ssDNA and the resulting stabilization effect on salt-induced aggregation). It was found that the PtNPs/rGO nanocomposites with 7 : 1

H_2PtCl_6-to-GO mass ratio had the highest catalytic activity. Compared with natural peroxidase, just like other nanomaterial-based enzyme mimetics, the PtNPs/rGO nanocomposites exhibited excellent thermal and pH stabilities. In addition to the oligo-nucleotide target, the versatility of this platform was demonstrated by PCR product detection. Taken together, this new platform is promising for point-of-care and on-site nucleic acid testing. Moreover, by using aptamer probes, this method can be readily applied to a broad spectrum of non-nucleic acid analytes, including ions, small molecules, and proteins.

Acknowledgements

References

1 L. Gao, J. Zhuang, L. Nie, J. Zhang, Y. Zhang, N. Gu, T. Wang, J. Feng, D. Yang, S. Perrett and X. Yan, *Nat. Nanotechnol.*, 2007, **2**, 577–583.

2 H. Wei and E. Wang, *Anal. Chem.*, 2008, **80**, 2250–2254.

3 L. Gao, J. Wu, S. Lyle, K. Zehr, L. Cao and D. Gao, *J. Phys. Chem. C*, 2008, **112**, 17357–17361.

4 F. Yu, Y. Huang, A. J. Cole and V. C. Yang, *Biomaterials*, 2009, **30**, 4716–4722.

5 Z. Zhang, Z. Wang, X. Wang and X. Yang, *Sens. Actuators, B*, 2010, **147**, 428–433.

6 M. Liang, K. Fan, Y. Pan, H. Jiang, F. Wang, D. Yang, D. Lu, J. Feng, J. Zhao, L. Yang and X. Yan, *Anal. Chem.*, 2013, **85**, 308–312.

7 H. Wei and E. Wang, *Chem. Soc. Rev.*, 2013, **42**, 6060–6093.

8 Y. Lin, J. Ren and X. Qu, *Acc. Chem. Res.*, 2014, **47**, 1097–1105.

9 A. Asati, S. Santra, C. Kaittanis, S. Nath and J. M. Perez, *Angew. Chem., Int. Ed.*, 2009, **48**, 2308–2312.

10 C. Xu, Z. Liu, L. Wu, J. Ren and X. Qu, *Adv. Funct. Mater.*, 2014, **24**, 1624–1630.

11 M. I. Kim, K. S. Park and H. G. Park, *Chem. Commun.*, 2014, **50**, 9577–9580.

12 Y. Song, X. Wang, C. Zhao, K. Qu, J. Ren and X. Qu, *Chem. – Eur. J.*, 2010, **16**, 3617–3621.

13 Y. Song, K. Qu, C. Zhao, J. Ren and X. Qu, *Adv. Mater.*, 2010, **22**, 2206–2210.

14 Y. Jv, B. Li and R. Cao, *Chem. Commun.*, 2010, **46**, 8017–8019.

15 Z. Gao, M. Xu, L. Hou, G. Chen and D. Tang, *Anal. Chim. Acta*, 2013, **776**, 79–86.

4082 | *J. Mater. Chem. B*, 2016, **4**, 4076–4083

This journal is © The Royal Society of Chemistry 2016

16 G.-W. Wu, S.-B. He, H.-P. Peng, H.-H. Deng, A.-L. Liu, X.-H. Lin, X.-H. Xia and W. Chen, *Anal. Chem.*, 2014, **86**, 10955–10960.

17 W. Li, H. Zhang, J. Zhang and Y. Fu, *Anal. Methods*, 2015, **7**, 4464–4471.

18 Y. Ju and J. Kim, *Chem. Commun.*, 2015, **51**, 13752–13755.

19 N. Wang, B. Li, F. Qiao, J. Sun, H. Fan and S. Ai, *J. Mater. Chem. B*, 2015, **3**, 7718–7723.

20 W. He, Y. Liu, J. Yuan, J.-J. Yin, X. Wu, X. Hu, K. Zhang, J. Liu, C. Chen, Y. Ji and Y. Guo, *Biomaterials*, 2011, **32**, 1139–1147.

21 H. Chen, Y. Li, F. Zhang, G. Zhang and X. Fan, *J. Mater. Chem.*, 2011, **21**, 17658–17661.

22 M. Liu, H. Zhao, S. Chen, H. Yu and X. Quan, *ACS Nano*, 2012, **6**, 3142–3151.

23 Y. Zhang, C. Xu, B. Li and Y. Li, *Biosens. Bioelectron.*, 2013, **43**, 205–210.

24 M. I. Kim, M. S. Kim, M.-A. Woo, Y. Ye, K. S. Kang, J. Lee and H. G. Park, *Nanoscale*, 2014, **6**, 1529–1536.

25 L.-N. Zhang, H.-H. Deng, F.-L. Lin, X.-W. Xu, S.-H. Weng, A.-L. Liu, X.-H. Lin, X.-H. Xia and W. Chen, *Anal. Chem.*, 2014, **86**, 2711–2718.

26 H. Wang, S. Li, Y. Si, N. Zhang, Z. Sun, H. Wu and Y. Lin, *Nanoscale*, 2014, **6**, 8107–8116.

27 J. Qian, X. Yang, Z. Yang, G. Zhu, H. Mao and K. Wang, *J. Mater. Chem. B*, 2015, **3**, 1624–1632.

28 Y. Sun, J. Wang, W. Li, J. Zhang, Y. Zhang and Y. Fu, *Biosens. Bioelectron.*, 2015, **74**, 1038–1046.

29 X.-Q. Lin, H.-H. Deng, G.-W. Wu, H.-P. Peng, A.-L. Liu, X.-H. Lin, X.-H. Xia and W. Chen, *Analyst*, 2015, **140**, 5251–5256.

30 C.-H. Lu, H.-H. Yang, C.-L. Zhu, X. Chen and G.-N. Chen, *Angew. Chem., Int. Ed.*, 2009, **48**, 4785–4787.

31 Y. Guo, L. Deng, J. Li, S. Guo, E. Wang and S. Dong, *ACS Nano*, 2011, **5**, 1282–1290.

32 M.-J. Li, C.-M. Liu, Y.-B. Xie, H.-B. Cao, H. Zhao and Y. Zhang, *Carbon*, 2014, **66**, 302–311.

33 J. D. Qiu, G. C. Wang, R. P. Liang, X. H. Xia and H. W. Yu, *J. Phys. Chem. C*, 2011, **115**, 15639–15645.

34 M.-Y. Yen, C.-C. Teng, M.-C. Hsiao, P.-I. Liu, W.-P. Chuang, C.-C. M. Ma, C.-K. Hsieh, M.-C. Tsai and C.-H. Tsai, *J. Mater. Chem.*, 2011, **21**, 12880–12888.

35 S. Guo, D. Wen, Y. Zhai, S. Dong and E. Wang, *ACS Nano*, 2010, **4**, 3959–3968.